
ESTIMATING THE NUMBER OF HTTP/3 RESPONSES IN QUIC USING DEEP LEARNING

Barak Gahtan¹, Robert J. Shahla¹, Reuven Cohen¹, Alex M. Bronstein¹

¹Technion Israel Institute of Technology, Haifa, Israel

{barakgahtan, shahlarobert, rcohen, bron}@cs.technion.ac.il

ABSTRACT

QUIC, a new and increasingly used transport protocol, enhances TCP by providing better security, performance, and features like stream multiplexing. These features, however, also impose challenges for network middle-boxes that need to monitor and analyze web traffic. This paper proposes a novel solution for estimating the number of HTTP/3 responses in a given QUIC connection by an observer. This estimation reveals server behavior, client-server interactions, and data transmission efficiency, which is crucial for various applications such as designing a load balancing solution and detecting HTTP/3 flood attacks.

The proposed scheme transforms QUIC connection traces into a sequence of images and trains machine learning (ML) models to predict the number of responses. Then, by aggregating images of a QUIC connection, an observer can estimate the total number of responses. As the problem is formulated as a discrete regression problem, we introduce a dedicated loss function. The proposed scheme is evaluated on a dataset of over seven million images, generated from 100,000 traces collected from over 44,000 websites over a four-month period, from various vantage points. The scheme achieves up to 97% cumulative accuracy in both known and unknown web server settings and 92% accuracy in estimating the total number of responses in unseen QUIC traces.

1 Introduction

Quick UDP Internet Connections (QUIC) Iyengar and Thomson (2021) is gradually replacing TCP as the main internet transport protocol due to its enhanced security and performance. Stream multiplexing is one of the most important features of QUIC. It allows an HTTP Bishop (2022) server to send the client several HTTP objects simultaneously, one on each stream, while avoiding head-of-the-line blocking.

The data in each stream is carried by different QUIC frames. Every QUIC packet can carry multiple frames, each containing data belonging to a different object. Since the various streams are independent of each other, when a stream is delayed due to a packet loss, there is no impact on the progress of the other streams Bishop (2022); Kühlewind and Trammell (2022). HTTP/3 is a mapping of HTTP semantics over QUIC. HTTP/3 communication over QUIC streams is performed using requests and responses, such that each request is allocated a stream from the client to the server, and each response is allocated a stream from the server to the client Bishop (2022).

This paper considers an observer listening to the channel between the QUIC client and server. **This observer sees the data packets sent in both directions and aims to estimate the number of objects this connection carries.** This information can be useful for various applications. The most important application is HTTP/3 load balancing. A load balancer can successfully balance the load it assigns to different machines if it is able to estimate the load imposed by each connection Shahla et al. (2024). This is difficult with HTTP/3, because the load balancer does not know how many requests are sent by a client to the server on different QUIC streams¹. The scheme presented in this paper can help to address this problem.

¹This is also difficult with HTTP/2, because multiple requests can also be sent by an HTTP/2 client over one TCP connection. In this case, different streams are implemented by HTTP and not by QUIC. The same approach proposed here for HTTP/3 over QUIC is applicable for HTTP/2 over TCP.

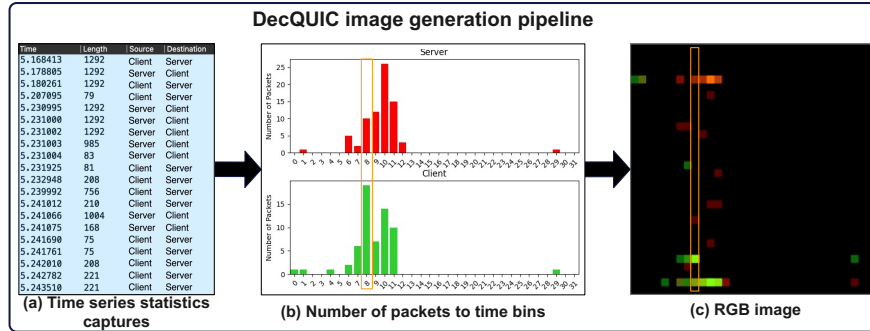


Figure 1: Generation of an image representing observed QUIC packets. The captured connection trace is windowed into overlapping temporal intervals. In each temporal window, the number of packets sent by the client and the server are binned into time bins. The obtained two-dimensional histograms (number of packets vs. time) are represented as an RGB image, with the green channel representing the packets sent by the client, the red channel representing the packets sent by the server, and the blue channel being unused.

Another use case is detecting HTTP/3 flood attack Chatzoglou et al. (2023). In this attack, multiple HTTP/3 requests were sent to the server over a single connection. As indicated in Chatzoglou et al. (2023), identifying such an attack is challenging, because the attack pattern is almost identical to that of the normal traffic.

This paper presents a new scheme called DecQUIC, which can be used by an observer to estimate the number of request/response pairs in a QUIC connection. To train this scheme, we extend the work of Horowicz et al. (2022); Shapira and Shavitt (2019). A QUIC connection trace is first captured and divided into multiple window times. Then, for each window, two histograms are generated: the first describes the number of packets sent by the client during this window, and the second describes the number of packets sent by the server during this window. These histograms are used, together with information about the length and time of each packet and density, to generate an RGB image. In this image, the red channel represents the normalized number of packets sent by the server, the green channel represents the normalized number of packets sent by the client during the corresponding time window, and the blue channel is not used. The above process is illustrated by Figure 1. As mentioned, visualizing traffic flows as images was introduced in Shapira and Shavitt (2019), but their images were grayscale with a single channel, and contained no information about packet density. Therefore, it is insufficient for the task of predicting the number of HTTP/3 responses. The single-channel approach offers only a broad traffic overview, limiting its ability to distinguish between client-to-server and server-to-client. This is crucial in QUIC, where HTTP/3 requests and responses involve multiplexed streams. Moreover, QUIC’s complexity, (stream multiplexing and independent packet handling), requires separate analysis of traffic directions.

After the above scheme transforms a QUIC trace into a sequence of RGB images representing the connection, a ML model is trained to receive a single image and predict the number of HTTP/3 responses that start in each image during every time window. This scheme works both online and offline. In the former case, it estimates the number of responses sent by the server rapidly for a predetermined short period of time (for example, the first 100ms of a connection). In the latter case, it estimates the total load imposed on a server during a long period of time. The considered problem is not a classic classification task because the misclassification errors depend on the distance between the real number of responses and the predictions. It is also not a standard regression task, as the numbers of responses are discrete. We, therefore, formulate a discrete regression task and develop a special loss function for it.

To train and evaluate DecQUIC, we introduce a labeled dataset comprising over 100,000 QUIC traces from more than 44,000 websites (URLs), collected over a four-month period, from various vantage points. These traces provide the foundation for generating more than two million images, which were configured based on window length, pixel resolution, and normalization. We demonstrate that DecQUIC can achieve up to 97% accuracy when utilizing images with time windows of $T = 0.1$ or $T = 0.3$ seconds. The flexibility of the dataset allows for configurable analysis at different granularities, showcasing the utility of QUIC traces in performance evaluation.

The rest of this paper is organized as follows: Section 2 reviews related work. Section 3 describes the proposed deep learning (DL) scheme and its challenges. Section 4 discusses the proposed loss function used for training the ML models. Section 5 presents an evaluation of the trained ML models on out-of-training sample QUIC traces and out-of-distribution sample web servers. Section 6 uses the trained ML models to estimate the number of HTTP/3 responses over complete QUIC traces. Finally, Section 7 concludes the paper.

2 Related Work

The rise of encrypted traffic in recent years has led to a marked increase in the adoption of flow-based techniques that depend on ML for the analysis of statistical or time series data. Among these techniques are k -Nearest Neighbors (KNN), Random Forest (RF), Naive Bayes (NB), and Support Vector Machines (SVM) Pacheco et al. (2020); Sun et al. (2010); Velan et al. (2015). DL and deep neural network (NN) techniques have surfaced more recently for the classification of encrypted communications Lotfollahi and Siavoshani (2020); Wang et al. (2018).

The authors in Tong and Tran (2018) proposed a two-stage traffic classification approach using RF and convolutional neural networks (CNN), demonstrating high accuracy (up to 99%) across various QUIC-based services. In another work Rezaei and Liu (2020), the authors developed a multi-task traffic classification technique using CNN that predicted bandwidth requirements, flow duration, and traffic class, outperforming single-task and transfer learning approaches with up to 90% accuracy on ISCX Ghorbani et al. (2012) and QUIC Chadi Assi (2020) public datasets. The same authors later proposed a semi-supervised method using CNN that showed potential even when trained on a small dataset. Their work differs from ours in two major ways. To begin, their method is trained and evaluated only on Google’s services using Google web servers, as opposed to ours, which is trained and evaluated on many different web servers. Second, they classify the type of service rather than the characteristics of the QUIC connection itself.

In Almuhammadi et al. (2023), the authors addressed the difficulties presented by encrypted traffic using five different ensemble ML techniques: RF, Extra Trees, Gradient Boosting Tree, Extreme Gradient Boosting Tree (XGBoost), and the Light Gradient Boosting Model (LGBM). They assessed these ML models using a publicly accessible dataset and found that XGBoost and LGBM perform particularly well in terms of high accuracy and efficiency when it comes to classifying encrypted QUIC traffic. Their dataset includes five distinct QUIC traffic types that were created specifically for ML classification using only the Google web server, whereas ours includes many web servers and over 72,000 distinct traces.

The authors in Secchi and Cassarà (2022) showed work utilizing SVM, KNN, RF, and NN models for encrypted traffic classification, demonstrating impressive results, with all models achieving over 97% accuracy on QUIC traffic. Their work, unlike ours, is intended for QUIC over satellite only, mitigating the different client-server behaviors among different web servers. In a different work, the authors in Towhid and Shahriar (2022) developed a self-supervised approach for encrypted network traffic classification that, despite having few labeled data, achieved 98% accuracy on the QUIC dataset, surpassing the baseline by 3%. Unlike us, the QUIC dataset only contains Google connections and its classification technique works exclusively on (numerous) Google services. We on the other hand, estimate certain characteristics of the connection itself.

In their work, the authors of Izadi et al. (2022a) devised a method to differentiate between VPN and non-VPN encrypted traffic using the ISCX VPN-non-VPN dataset. This approach combines the ant-lion meta-heuristic algorithm, the self-organizing map algorithm, and CNN for feature extraction and classification, yielding a high accuracy of 98% on the test data. Analogously, a separate study Izadi et al. (2022b) by the same authors employed data fusion methods and DL for traffic classification on the same dataset. Their classification, unlike ours, is whether it is a VPN or non-VPN data connection.

CESNET-QUIC22 (Luxemburk et al., 2023a) is a QUIC traffic dataset collected from backbone lines of a large Internet service provider. It contains over 153 million connections and 102 service labels, captured during one month.

In Luxemburk et al. (2023b), the authors demonstrate three techniques for QUIC service classification using the CESNET-QUIC22 dataset. They do not deal with out-of-distribution settings, in which web servers that were not present in the training set are visible during evaluation, whereas we do. Additionally, they classify services rather than connection characteristics. In Geiginger (2021) the CESNET-QUIC22 dataset was used once again to evaluate the effectiveness of various classification models, including a multi-modal CNN, LightGBM, and IP-based classifiers. Their study sets a new standard for fine-grained service classification within encrypted QUIC traffic, highlighting the models’ abilities to discern web services accurately in a secure and encrypted communication framework. The authors of Geiginger (2021) do not deal with out-of-distribution settings, in which web servers that were not present in the training set are visible during evaluation; we, however, do.

3 DecQUIC Framework

We consider an observer who can see the QUIC encrypted packets transmitted from the client to the server, and vice versa. For each packet, the observer knows its direction, length, and the observed time. DecQUIC uses this information to convert QUIC traces into representative colored images, which are then suitable for ML models to train on. To convert the captured QUIC traces into time-series data, the sliding window technique Frank et al. (2001) is

used. This technique requires two parameters: the window length and the overlap between consecutive windows. We show results for two different sliding window lengths, $T = 0.1$ and $T = 0.3$ seconds. During training, we use a 90% overlap between windows to increase the number of images. For evaluation, we use a 0% overlap to ensure the images represent the entire connection, allowing us to estimate the total responses in the connection, without double-counting responses.

Figure 1 shows an example of the construction steps for an image with a window length of 0.3 seconds from a trace. During step (a), some of the trace statistics are collected: the time when the observer sees this packet, the packet’s length, and the packet’s direction. Afterwards, each window is split into 32 time bins. For example, for a 0.3-second window, each bin contains 9.375 milliseconds of traffic. Step (b) shows histograms with $M = 32$ time bins for the considered window. The upper one is for the packets sent by the server, and the lower one is for packets sent by the client. The horizontal axis represents the time bins, and the vertical axis represents the number of packets received during each bin. For example, in the 8-th time bin (boxed in orange), the server sent 10 packets and the client sent 19 packets. Step (c) shows the image constructed for the considered example. The image represents the packet length statistics and the number of packets. Once the traces are captured, the image dataset generation process begins. For each trace, the SSL keys are stored in a separate file (and are included in the dataset), and then used to decrypt the relevant QUIC packets and determine the number of responses within each window (thereby labeling the images). The label for an image indicates the number of HTTP/3 responses the observer captured during the corresponding window.

Figure 2 shows an example of the constructed image. The image is constructed on an $M \times N$ equispaced grid. The horizontal dimension represents different time window locations, while the vertical dimension represents different packet lengths. Thus, each packet is binned into one of the $M \times N$ bins according to its length and time. In all our experiments, we choose $M = N = 32$ as a compromise between the image size and the image resolution. When fine bins are used, the increased image size increases the training and inference burden, but with little gain in accuracy. Coarser bins were observed to impair the model’s performance. Our tested values are 32, 64, 128 and 256, as further discussed in Horowicz et al. (2022).

In the resulting image, the pixel at location (i, j) represents the normalized number of packets whose length falls within the j -th bin received during the temporal span of the i -th time bin. The pixel’s RGB values represent the normalized number of packets (i.e., density) sent from the server to the client (red) and from the client to the server (green). The blue channel is unused. The time interval spanned by the i -th bin is $[i\Delta t, (i + 1)\Delta t)$, where $\Delta t = T/M$ and T denotes the window length. In our experiments, we used $T = 0.1$ and $T = 0.3$ seconds. To be counted in length bin j , the length of a packet should be in the range of $[j\Delta l, (j + 1)\Delta l]$ with $\Delta l = L/N$ and $L = 1,500$ bytes denoting the maximum transmission unit (MTU). Histogram counts are normalized per channel window-wise using min-max normalization Patro and Sahu (2015), $x_{\text{norm}} = (x - x_{\text{min}})/(x_{\text{max}} - x_{\text{min}})$, where x and x_{norm} are the original and normalized packet counts, respectively, and x_{min} and x_{max} are the minimum and maximum values of the packet count for the specific direction in the considered window, respectively. The normalized value is multiplied by 255 to fit an 8-bit image format. If there is no traffic for a specific window, all pixels will contain the value zero. Note that the shortest QUIC packet is longer than what is represented by the first length bin. Therefore, the first row of the image grid consistently exhibits pixels with a value of zero.

Figure 2 shows different densities for each channel. For example, during time bin $i = 7$, different shades of green are displayed. This indicates that the client sent packets of five different lengths, which fall into bins $j = 2, 6, 12, 27,$ and 28 . The five pixels are purely green, indicating that all the packets observed during bin $i = 7$ were sent by the client. The brightness of a pixel increases as its value approaches 255. Pixel $(7, 12)$ is the brightest across the whole window in the green channel and it represents 8 packets. This means that the largest number of packets sent by the client during the window is observed during time bin $i = 7$,

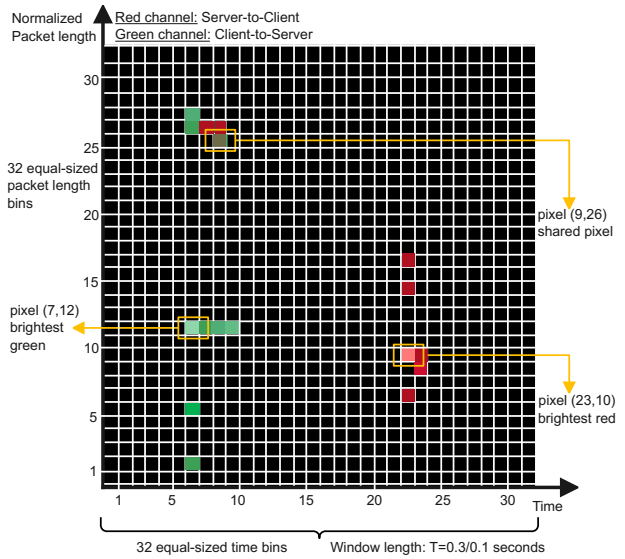


Figure 2: A DecQUIC image, representing QUIC connection activity. Pixel positions represent histogram bins (horizontal and vertical axes corresponding to time and packet length, respectively). The values of the red and green channels represent normalized, per-window, histogram counts of the response and request packets, respectively.

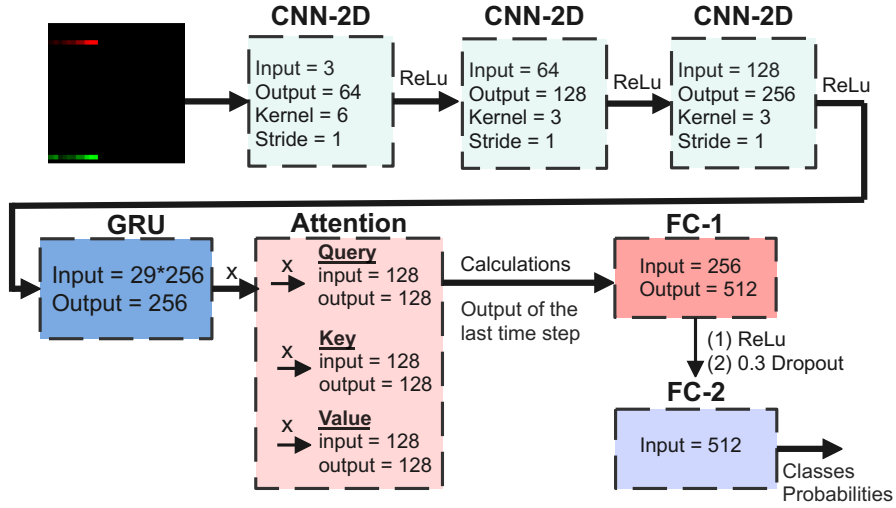


Figure 3: The proposed DecQUIC neural network architecture.

when their length fell in bin $j = 12$. The other green pixels represent between 2 to 5 packets that are sent by the client. At time bin $i = 23$, the server sent packets of four different lengths, which are classified, based on their length, into bins $j = 7, 10, 15$, and 17 . The four pixels are purely red, indicating that during time bin $i = 23$, only packets sent by the server are observed. Pixel $(23, 10)$, representing 18 packets, is the brightest within the red channel across the entire window. The rest of the red pixels represent between 3 and 15 packets sent by the server. Pixel $(9, 26)$ is a combination of green and red, indicating that during time bin $i = 9$, packets from both the client and the server are observed and their length puts them into bin $j = 26$.

DecQUIC’s image construction is an extension of the technique proposed by FlowPic Shapira and Shavitt (2019), which transforms network flows into images. FlowPic generates images based on packet lengths and their observed times, with the objective of constructing a grayscale image using a flow-based two-dimensional histogram. However, FlowPic’s single-channel approach, while providing a general traffic overview, is insufficient for more nuanced analysis, particularly in the context of QUIC. In QUIC, distinguishing between client-to-server and server-to-client traffic is critical due to the multiplexed nature of HTTP/3 requests and responses. Furthermore, QUIC’s inherent complexity—stemming from stream multiplexing and independent packet handling—necessitates a more detailed examination of traffic directions. For those reasons, DecQUIC introduces a separate channel for each direction between a client and a server, a density factor for the packets’ count in a given window, a configurable number of bins, and uses a very short time window per each image. The result is an RGB image.

The final step in transforming the task into an ML problem is the creation of a labeled image dataset, from over 100,000 traces collected from over 44,000 websites (URLs). Each image in this dataset represents a snapshot of network activity, labeled with the number of HTTP/3 responses that started to be seen by an observer for every time window. To this end, the HTTP/3 frames are analyzed using the SSL identified keys and HTTP/3 HEADERS frames.

Figure 3 shows the neural network (NN) architecture used in our experiments. The architecture is based on Ismail Fawaz et al. (2020); Khan et al. (2021). It includes CNN layers, a gated recurrent unit (GRU), and a self-attention mechanism. Each component plays a crucial role in the estimation task. The initial CNN layers extract spatial features from the input data. The first convolution layer uses 64 filters with a 6×6 kernel to capture low-level features such as rectangles representing packets arriving during consecutive bins. A 6×6 kernel in a 32×32 image enables the ML model to examine large sub-windows of the image, accounting for nearly 20% of the image size. A smaller 3×3 kernel in the first layer produced inferior results.

To process the low-level features and extract higher-level spatial information, the subsequent layers apply 128 and 256 filters with 3×3 kernel sizes, respectively. A ReLU activation is used after each convolutional layer to allow the model to learn more complex features Krizhevsky et al. (2012). The GRU layer processes the output of the convolutional layer, allowing it to detect temporal patterns in the images. Prior to feeding data into the GRU, we perform a reshaping operation to ensure the GRU layer correctly interprets the time dimension. This transformation preserves the temporal order of the data. Unlike traditional NNs, GRUs can learn long-term dependencies in sequential

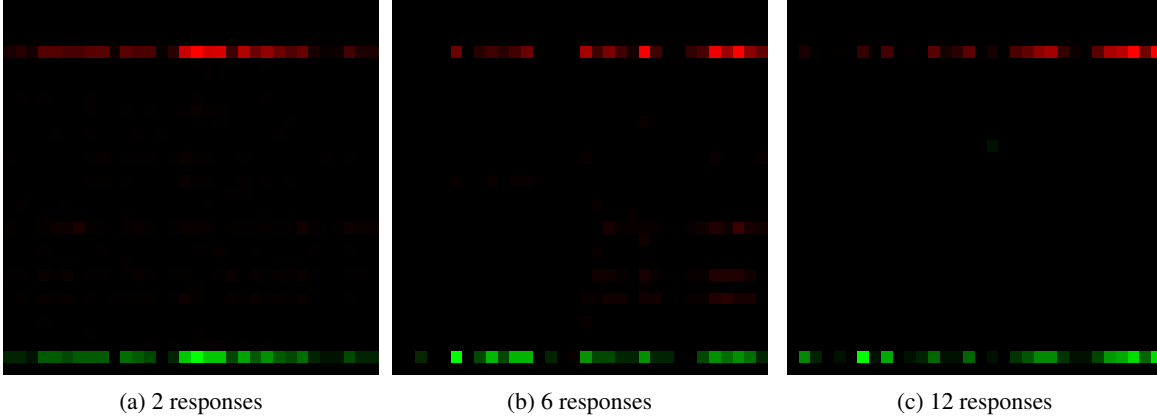


Figure 4: Three examples of DecQUIC image representation of QUIC flows with the number of HTTP/3 responses annotated next to each image. Note that visually similar images may have highly distinct labels.

data, which makes them ideal for time series tasks Dey and Salem (2017). Following the CNN and GRU layers, a self-attention mechanism is used. It is a crucial component of the architecture Vaswani et al. (2017), which enables ML models to focus on the most relevant input sequences. The self-attention module computes attention scores using the GRU output. It allows the ML models to weigh different parts of the sequence differently, thereby improving their ability to capture important temporal features. Finally, our architecture consists of two fully connected layers (FC-1 and FC-2) with ReLU activation, interspaced by a 0.3 dropout layer for regularization. The dropout layer helps to prevent overfitting and ensures that the model generalizes well to new data.

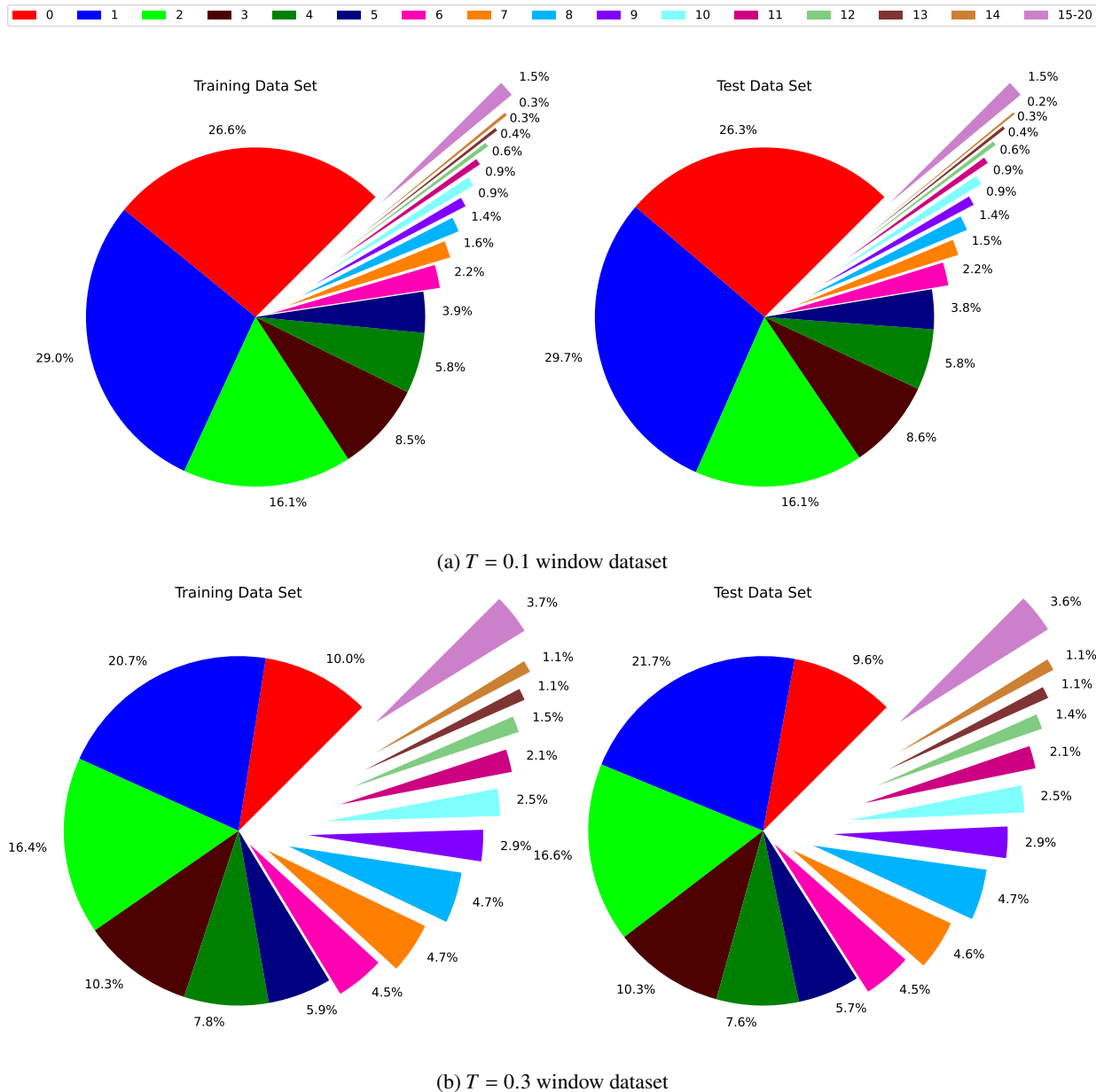
Once the task is formulated as an ML problem, the objective is to predict the number of HTTP/3 responses represented by each image. This task presents the following three challenges: (1) visually similar images are often assigned highly divergent labels; (2) the datasets (the $T = 0.1$ and $T = 0.3$ window datasets) are imbalanced, complicating the training process; and (3) the learning task deviates from conventional regression or classification models, which complicates both the training and evaluation processes. Through the rest of the paper, the term “class” is used to denote the number of responses associated with each image (the label).

Figure 4 illustrates the first challenge, visually distinguishing between images. It presents three images, each tagged with different labels. Figures 4(a), 4(b) and 4(c) show that although the images look similar, their class labels vary significantly. The server-to-client and client-to-server interaction patterns for images with these labels are strikingly similar. The packet density on the left side of the images is roughly the same, and the packet lengths fall into almost identical bins in both directions.

The second challenge is the distribution of classes per image within each dataset. Both datasets are significantly skewed. Figure 5(a) and Figure 5(b) display the distribution of classes for two window lengths. Notice the very rare cases of images with more than 15 HTTP/3 responses. As the figures demonstrate, images whose class values are 10 or more are also infrequent in both datasets. To mitigate class imbalance, we developed a dedicated loss function and implemented a data augmentation technique. Data augmentation enhances the representation of minority classes by increasing the diversity and quantity of samples, which helps to prevent the ML model from favoring the majority class.

The images are generated from QUIC traces that are formatted into a 32×32 pixel grid. Each pixel corresponds to a unique feature of network traffic over a specific period. Any disruption in the temporal dependencies present in each image, such as non-order-preserving modifications, may result in the loss of critical information, reducing the ML model’s ability to estimate correctly. Thus, data augmentation is only applied to the minority classes (classes whose values are between 10 and 20), incorporating a minimal noise level Maharana et al. (2022). We used noise with the standard deviation of $\sigma = 2.55$ corresponding to 1% of the pixel value, ensuring that the added noise does not drastically alter the image appearance or disrupt the temporal dependencies. The noise serves, however, to imitate minor variations, increasing the model’s robustness and generalization capabilities.

The third challenge is that the learning task cannot be categorized as a standard classification task or a standard regression task. Rather, it is a discrete regression problem. Consider, for example, an image with 17 responses. Estimating this number at 16 is better than estimating it at 15 or 19 because, unlike typical classification problems, the distance from the label is important. To address this issue, we developed a dedicated loss function that considers both

Figure 5: Dataset distributions for window lengths $T = 0.1$ and $T = 0.3$ seconds.

the imbalanced dataset and the desire to reward the model for correctly predicting classes that are closer to the actual label than those that are farther away. Section 4 explains the discrete regression loss function in more detail.

4 A Discrete Regression Loss Function

During the development of our model to accurately estimate the number of responses, we experimented with various conventional loss functions, each designed to address a specific aspect of the task. We first used the Cross-Entropy Loss, a standard method for classification problems, but it struggled with our dataset’s inherent class imbalance. We next considered the Mean Squared Error (MSE) Loss, and Mean Absolute Error (MAE) which are commonly used in regression tasks, but those did not properly consider the ordinal nature of our labels, and both operate for continuous labels when the labels in our case are discrete. Additionally, we tested the Huber Loss, which is robust to outliers and

combines the benefits of classification and regression loss functions, but it did not consider the need to preserve the ordinal sequence among the classes.

These limitations motivated the development of a new loss function that integrates the advantages of multiple approaches to better suit our needs. To address the challenges outlined in Section 3, the proposed loss function,

$$L = \alpha \text{FL} + (1 - \alpha) ((\beta \text{ORL} + (1 - \beta)\text{DBL}) .$$

It comprises an aggregate of three terms: (1) a *focused loss* (FL) term, intended to alleviate class imbalance by minimizing the relative loss for well-classified cases while emphasizing difficult-to-classify ones; (2) a *distance-based loss* (DBL) term penalizing the model according to the predicted class’s distance from the true label; and (3) an *ordinal regression loss* (ORL) term that introduces higher penalties for misclassifications that disrupt the natural ordinal sequence of the dataset, where lower class values occur more frequently.

The FL term Lin et al. (2017) builds on the weighted cross-entropy loss De Boer et al. (2005) by adding a focusing parameter, γ , which adjusts the influence of each sample on the training process based on the classification confidence. This parameter, γ , modifies the loss function by scaling the loss associated with each sample by $(1 - p_t)^\gamma$, where p_t is the predicted probability of the true class y . This scaling reduces the loss from easy examples (where p_t is high), thereby increasing it for hard, misclassified examples, focusing training efforts on samples where improvement is most needed. Accordingly, the term is:

$$\text{FL}(\mathbf{x}, \mathbf{y}) = \mathbb{E}_{(\mathbf{x}, \mathbf{y})} \left[-w(y) \cdot (1 - \hat{y}_y(\mathbf{x}))^\gamma \cdot \mathbf{y}^T \log \hat{\mathbf{y}}(\mathbf{x}) \right],$$

where \mathbf{x} denotes the input sample, \mathbf{y} is the one-hot encoded ground truth label, $\hat{\mathbf{y}}(\mathbf{x})$ represents the model’s output of class probabilities, $\hat{y}_y(\mathbf{x})$ denotes the predicted probability of the true class y , and $w(y)$ is a weight inversely proportional to the class frequency of y in the training dataset. By assigning a higher weight to less frequent classes, the model places more emphasis on accurately classifying these classes during training. It is an effective strategy for dealing with class imbalance Aurelio et al. (2019); Tian et al. (2020); Lin et al. (2017). FL thus minimizes the relative loss for well-classified examples, while emphasizing difficult-to-classify ones.

The DBL term Wang et al. (2020)

$$\text{DBL} = \mathbb{E}_{(\mathbf{x}, \mathbf{y})} \left[\sum_i \hat{y}_i(\mathbf{x}) \cdot |i - y| \right],$$

with y denoting the ground truth class, is essentially a discrete regression loss that penalizes the model’s output according to the predicted class’s distance from the true label. The distance is computed as the absolute difference between the class indices and the target class.

Finally, the ORL term Rennie and Srebro (2005); Frank and Hall (2001) is given by

$$\text{ORL} = \mathbb{E}_{(\mathbf{x}, \mathbf{y})} \left[-\mathbf{y}^T \log \sigma(\hat{\mathbf{y}}) - (1 - \mathbf{y})^T \log \sigma(1 - \hat{\mathbf{y}}) \right],$$

with σ denoting the sigmoid function saturating the input between 0 and 1. ORL uses a binary cross-entropy loss function, which compares the activation of each output neuron to a target that shows if the true class is greater than or equal to each class index, thus helping the model determine the order of the classes. Both DBL and ORL consider the relations between classes; they do so in different ways: DBL penalizes predictions based on the numerical distance, while ORL makes explicit use of the classes’ order. It focuses on preserving the correct order among predictions rather than the numerical distance between them.

The parameters α , β , and γ in the aggregated loss are used to balance the contributions of these three components to the combined loss. α is a parameter that controls the balance between the FL term and the ORL and DBL combination. A higher value of α gives more weight to the FL term, while a lower value gives more weight to the ORL and DBL combination. β is a parameter that controls the balance between the ORL and DBL terms. A higher value of β gives more weight to the ORL term, while a lower value gives more weight to the DBL term. γ is a parameter used inside the FL component to adjust the focusing effect of the FL term. A higher γ increases the effect of the focusing mechanism. This means the model pays more attention to correcting its worst mistakes, which is useful in highly imbalanced scenarios. Lower γ values reduce the impact, making the loss more like a standard cross-entropy loss where each misclassification is weighted more uniformly.

In Section 5, we present an ablation study on the terms of the proposed loss function, demonstrating the importance of each term for achieving the best performance.

5 Evaluating the Machine Learning Models

We now present a quantitative evaluation of the proposed framework in two settings: when the web servers are known to the observer, and when they are not. In the former case, a set of models were trained and evaluated exclusively on

Table 1: Summary statistics of QUIC traces and the number of images per dataset for each web server. Each web server containing multiple websites (URLs).

| Web Server | Websites | Traces | $T = 0.1$ | $T = 0.3$ |
|--------------------|----------|--------|-----------|-----------|
| youtube.com | 399 | 2,109 | 139,889 | 54,659 |
| semrush.com | 1,785 | 9,489 | 474,716 | 221,477 |
| discord.com | 527 | 7,271 | 623,823 | 235,248 |
| instagram.com | 3 | 207 | 17,003 | 7,112 |
| mercedes-benz.com | 46 | 66 | 9,987 | 2,740 |
| bleacherreport.com | 1,798 | 8,497 | 781,915 | 331,530 |
| nicelocal.com | 1,744 | 1,666 | 148,254 | 48,900 |
| facebook.com | 13 | 672 | 25,919 | 10,988 |
| pcmag.com | 5,592 | 13,921 | 1,183,717 | 385,797 |
| logitech.com | 177 | 728 | 56,792 | 28,580 |
| google.com | 1,341 | 2,149 | 81,293 | 29,068 |
| cdnetworks.com | 902 | 2,275 | 207,604 | 85,707 |
| independent.co.uk | 3,340 | 3,453 | 176,768 | 68,480 |
| cloudflare.com | 26,738 | 44,700 | 1,347,766 | 341,488 |
| jetbrains.com | 35 | 1,096 | 34,934 | 18,470 |
| pinterest.com | 43 | 238 | 6,465 | 2,360 |
| wiggle.com | 4 | 0 | 0 | 0 |
| cnn.com | 27 | 2,127 | 91,321 | 59,671 |

the QUIC traces pertaining to the web servers assumed at inference time. In the latter case, a leave-two-servers-out evaluation was performed. We opted to conduct a leave-two-servers-out evaluation instead of a leave-one-server-out evaluation due to the presence of 18 web servers. Our intention is to reserve approximately 10% of the data for out-of-distribution evaluation. More details about the training and test set constructions are provided later in this section.

In both settings, different models were trained with windows of $T = 0.1$ and $T = 0.3$ seconds. They were all trained on 18 different web servers, with 44,000 websites and 100,000 traces that were captured over a four-month period. Table 1 provides summary statistics per web server; more detailed statistics broken down per web server for each class are provided in the Appendix. Classes with labels non-superior to 20 constitute 90% of the traces in the $T = 0.3$ -second window dataset and 95% of the traces in the $T = 0.1$ -second window dataset. Due to their scarceness (e.g., only 0.003% of the images are labeled as class 21.), classes above 20 were excluded from the training and test sets.

5.1 Results for Known Web Servers

First, we consider the case when the web servers are known to the observer monitoring the connection. Each web server’s traces were randomly split into training and test sets using the 80 : 20 ratio, ensuring out-of-training-sample evaluation. We performed five random splits, each time training a new ML model. The training was performed with a batch size of 64 images using the Adam optimizer Kingma and Ba (2014) with the ReduceLROnPlateau learning rate scheduler. When a plateau in validation loss is detected, the scheduler applies a 30% reduction in the learning rate, allowing for more fine-tuned modifications as the training advances. To reduce the risk of overfitting, an early stopping technique was used, with a patience parameter of six epochs (i.e., the training was stopped whenever the validation loss did not improve for six consecutive epochs). A grid search was performed to find the optimal values of α , β , and γ (of the loss function). The values considered were $\alpha \in \{0, 0.3, 0.5, 0.7, 1\}$, $\beta \in \{0, 0.4, 0.6, 1\}$, and $\gamma \in \{1, 2, 3\}$. This grid search also allowed us to systematically evaluate the impact of each parameter on the model’s performance. The optimal combination was chosen based on the lowest validation loss seen during the training process. The optimal values for $T = 0.3$ seconds were found to be $\alpha = 0.7$, $\beta = 0.4$, and $\gamma = 2$, while for $T = 0.1$ seconds, $\gamma = 3$ produced the best results with the same values of α and β .

The box plot in Figure 6 illustrates the accuracy of predicting the correct classes on out-of-training sample traces with windows of lengths $T = 0.1$ and $T = 0.3$ seconds, for one of the five iterations. The horizontal axis represents true labels, while the vertical axis represents predicted labels belonging to one of the 21 discrete classes. The vertical boxes show the 25-th, 50-th, and 75-th percentiles for each class prediction. In Figure 6(a) for the lower value classes (classes 0, 1 and 2), the rectangles appear as single lines, indicating minimal variation in the predicted values. This shows that the model’s predictions for these classes are consistently close to their true values. As the true labels increase in value, however, the rectangles widen, reflecting an increased prediction error variance.

Figure 6(b) demonstrates the same trends with the $T = 0.3$ -second window. Nevertheless, this model differs in two key points. Firstly, its accuracy for lower class values is higher and extends to class values of 4 rather than up to 2.

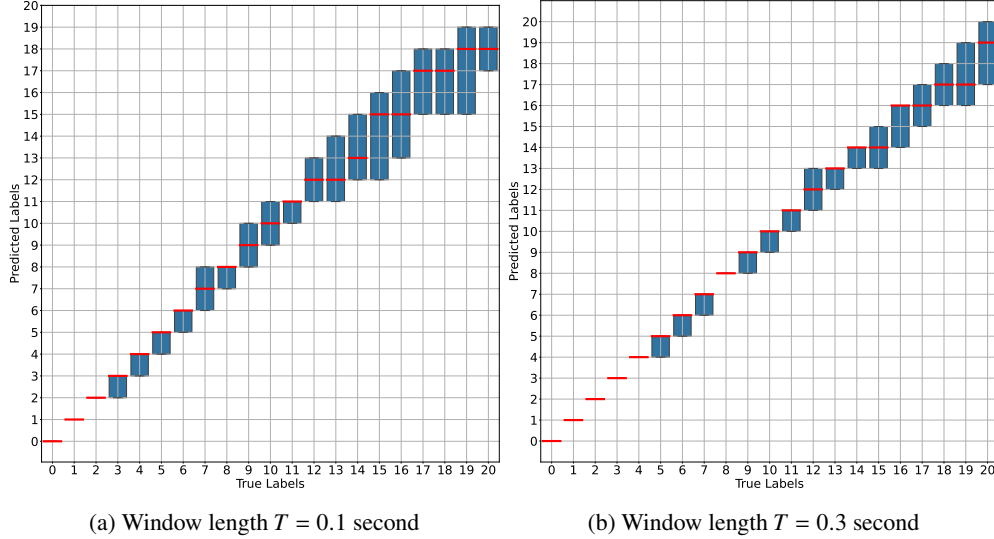


Figure 6: Prediction errors assuming known web servers. Red lines indicate the median predicted value; blue boxes show the 25 – 75% confidence intervals (iteration 1).

Table 2: CAP results for known web server setting, for five randomly selected splits of training and test sets using $T = 0.1$ and $T = 0.3$ window length datasets.

| Iteration | $T = 0.1$ | | $T = 0.3$ | |
|-----------|-----------|---------|-----------|---------|
| | ± 1 | ± 2 | ± 1 | ± 2 |
| 1 | 0.93 | 0.97 | 0.91 | 0.96 |
| 2 | 0.92 | 0.96 | 0.90 | 0.97 |
| 3 | 0.93 | 0.98 | 0.91 | 0.95 |
| 4 | 0.94 | 0.97 | 0.92 | 0.93 |
| 5 | 0.91 | 0.96 | 0.92 | 0.94 |

Secondly, the model demonstrates improved accuracy at the upper-class values (16 – 20). The prediction distributions are tighter and tend to be less biased. The enhanced performance observed with a $T = 0.3$ -second window is attributed to the dataset’s distribution (Figure 5). In the $T = 0.1$ -second window dataset, labels 0, 1 and 2 make up roughly 75% of the data, with the higher classes being represented in smaller proportions. Conversely, in the $T = 0.3$ -second window dataset, there is a more even distribution, with labels 0, 1 and 2 comprising only about 47% of the total dataset. For an online use case, a $T = 0.3$ -second window is a better choice for an observer to use, as every image is considered standalone.

Additionally, we introduce a Cumulative Accuracy Profile (CAP) metric, which provides a refined measure of classification accuracy by incorporating a tolerance level for each prediction. Unlike traditional metrics such as confusion matrices that require exact matches between predicted and true labels, CAP allows for a specified degree of tolerance, accommodating predictions that are close to the correct class. Formally, it is defined as:

$$\text{CAP}_{\pm k}(\mathbf{y}, \hat{\mathbf{y}}) = \frac{1}{n} \sum_{i=1}^n \mathbb{1}(|y_i - \hat{y}_i| \leq k),$$

where \mathbf{y} represents the vector of true class labels, $\hat{\mathbf{y}}$ denotes the model’s predictions, k specifies the tolerance level (e.g., ± 1 or ± 2 classes), n is the total number of samples, and $\mathbb{1}(\cdot)$ is the indicator function that evaluates to 1 if the condition is met and 0 otherwise. This metric thus quantifies the proportion of samples where the model’s predictions fall within the allowed tolerance around the true class. For example, a CAP score of 91% within a tolerance of ± 1 means that 91% of the predictions are at most one class away from the correct label.

For the models trained using both datasets, $T = 0.1$ and 0.3 second window dataset, the CAP results are presented in Table 2. We did not perform stratified sampling for the classes.

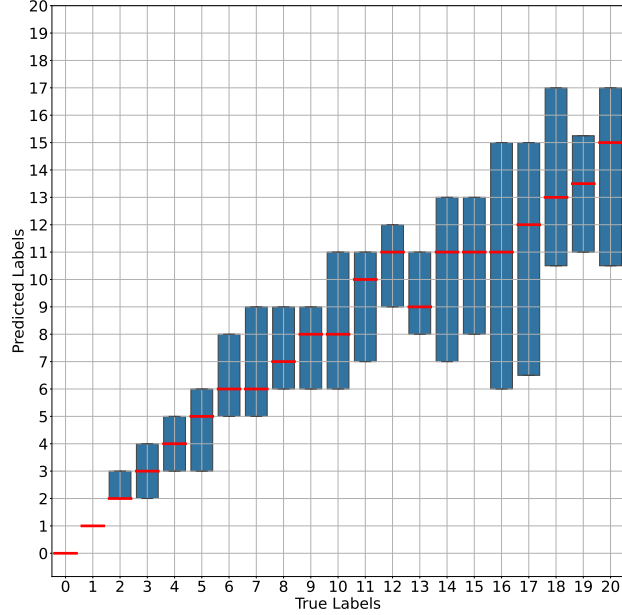


Figure 7: Prediction errors assuming unknown web servers. The testing servers are “independent.co.uk” and “google.com”, using a window length of $T = 0.3$ seconds. Red lines indicate the median predicted value; blue boxes show the 25-75% confidence intervals.

Table 3: CAP results for unknown web server setting, for ten randomly selected iterations of two web servers used for testing and the remaining for training, using the $T = 0.3$ window length dataset.

| Testing Servers | ± 1 | ± 2 |
|------------------------------------|---------|---------|
| bleacherreport.com, cloudflare.com | 0.62 | 0.76 |
| facebook.com, cdnetworks.com | 0.59 | 0.72 |
| logitech.com, mercedes-benz.com | 0.66 | 0.77 |
| bleacherreport.com, semrush.com | 0.63 | 0.75 |
| independent.co.uk, google.com | 0.83 | 0.90 |
| cnn.com, facebook.com | 0.82 | 0.88 |
| discord.com, youtube.com | 0.66 | 0.84 |
| discord.com, google.com | 0.61 | 0.80 |
| discord.com, independent.co.uk | 0.83 | 0.88 |
| bleacherreport.com, google.com | 0.78 | 0.85 |

5.2 Results for Unknown Web Servers

In the following, we present evaluation results for the unknown web server setting, in which the observer has no prior knowledge of which web servers to monitor. The task is to investigate if it is possible to learn on one set of web servers and do the evaluation on another. As client-server dynamics can vary across different web servers, this task essentially evaluates the model’s out-of-distribution performance. To achieve this, both datasets are divided into ten randomly selected combinations of web servers, with two reserved for testing and the remaining for training. The combination of training and testing web servers has a significant impact on the learning process’s results due to the class distribution across the datasets. For example, if the “semrush.com” web server is in the testing set but not in the training set, the majority of the higher value classes will be left out of training for this combination of web servers. This makes it difficult for an ML model to generalize effectively for unseen images for the higher-value classes. Furthermore, if we select web servers that do not have any higher-value class images (such as “instagram.com” or “pcmag.com”), the ML model will not be able to estimate higher-value classes. The paper does not include image statistics per web server due to space constraints. All models were trained using the same method as in the previously described experiments; in each iteration, a different model was trained and evaluated.

The box plot in Figure 7 depicts one of the ten iterations for the $T = 0.3$ -second window dataset. For this iteration, “independent.co.uk” and “google.com” were picked at random as the testing web servers, and the remaining web servers were used for training. Figure 7 shows that for the lower value classes (0 – 1), the model’s predictions are

Table 4: CAP results for unknown web servers setting, for ten randomly selected iterations of two web servers used for testing and the remaining for training, using the $T = 0.1$ -second window length dataset.

| Testing Servers | ± 1 | ± 2 |
|-----------------------------------|---------|---------|
| jetbrains.com, semrush.com | 0.69 | 0.78 |
| pcmag.com, discord.com | 0.86 | 0.94 |
| instagram.com, cloudflare.com | 0.79 | 0.90 |
| instagram.com, bleacherreport.com | 0.78 | 0.87 |
| youtube.com, jetbrains.com | 0.86 | 0.92 |
| pcmag.com, cloudflare.com | 0.80 | 0.89 |
| facebook.com, nicelocal.com | 0.75 | 0.85 |
| cdnetworks.com, independent.co.uk | 0.71 | 0.81 |
| cnn.com, facebook.com | 0.86 | 0.90 |
| youtube.com, nicelocal.com | 0.81 | 0.87 |

very accurate. For mid-range class values (2 – 12), the model’s predictions are within an acceptable tolerance level of ± 2 , while for the higher-value classes, the performance, clearly, has deteriorated. This is illustrated by a clear trend wherein predictions spread more widely in higher-value classes. The CAP results’ accuracy is 83% at ± 1 tolerance and 90% at ± 2 tolerance. Table 3 provides additional CAP results for each iteration.

Using a similar method, we evaluated the $T = 0.1$ -second window dataset, randomly choosing a pair of web servers for testing while the remaining web servers were used for training. The obtained results were similar to those using the $T = 0.3$ -window dataset, where the different ML models predicted the lower values with very high accuracy, but for the mid- and high-range class values, the predictions were more spread out. Table 4 provides additional CAP results for each iteration.

6 Evaluating on Complete Traces

This section presents results for estimating the total number of HTTP/3 responses in a trace. For this evaluation, **new images were generated with no overlap between the windows**, using the same test traces that were used before (Section 5, iteration 1, known web server scenario). The images were fed sequentially through the trained models, whose predictions were summed and compared to the sums of the trace’s true label.

Figure 8 shows prediction results on the same traces used in Section 5, using the $T = 0.1$ - and $T = 0.3$ -second subdivisions. The same traces were used to create the images. Both figures present a scatter plot in which the parameter θ , ranging between 0 and 1, modulates the transparency of the plot. At $\theta = 0$, a point placed in the plot is fully transparent, whereas at $\theta = 1$, it is opaque. In these plots θ is set to 0.05 to ensure high transparency and optimize the visual distinction between areas of high and low point density in cases of significant overlap among the roughly 12,000 data points in each plot. In this plot, each point represents the summed labels or predictions over the images of a trace. For example, if a trace is composed of five non-overlapping images whose true labels are 1, 0, 2, 4 and 1, then the true label of that trace is 8; if the model’s predictions are 1, 0, 3, 4 and 1, for the same images, then the summed prediction is 9, and that trace is represented in the plot as the (8, 9) point, with $\theta = 0.05$ density. If another trace has the same aggregated values and is placed at the same (8, 9) point, then it is placed on top of the previous point, thus making that point darker.

Figure 8(a) illustrates the scatter plot for predictions from the ML model trained using $T = 0.1$ -second window images, while Figure 8(b) displays results for $T = 0.3$ -second window. The test dataset includes 12,520 traces with an average of 21.2 images per trace for $T = 0.1$ -second window images and 12,142 traces with an average image of 7.5 per trace for $T = 0.3$ seconds. The figures highlight significant improvements in the performance of the two ML models: first, the $T = 0.3$ -second ML model (that was trained using the $T = 0.3$ window dataset) has 71% of predictions within ± 3 of a perfect prediction, whereas the $T = 0.1$ -second model achieves 92.6%, demonstrating a nearly 20% improvement in accuracy across entire traces. We use a ± 3 tolerance level because for both window lengths, the points represent the aggregated prediction sum and, thus, the aggregated errors as well. Therefore, a higher tolerance level is required since the average number of images per trace is 7.5 and 21.2 for the $T = 0.3$ -second and $T = 0.1$ -second, respectively. Secondly, the predictions of the model that was trained using a $T = 0.1$ -second window are notably more aligned along the diagonal, showing less deviation compared to those of the model that was trained using a $T = 0.3$ -second window, suggesting that finer timing resolutions enhance the performance for the cumulative prediction.

Figures 8(a) and 8(b) illustrate a notable difference in predictive behavior between models that were trained and evaluated with $T = 0.3$ - and $T = 0.1$ -second window sizes. Specifically, they show the presence of diagonal patterns

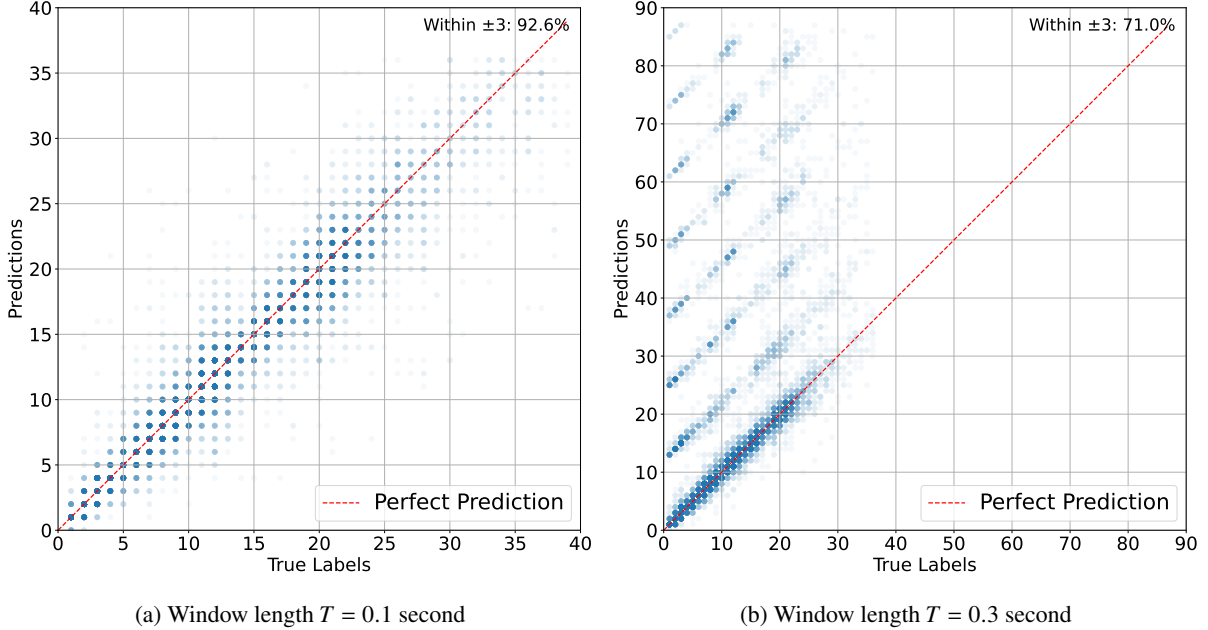


Figure 8: Scatter plots demonstrating the predictive results, where each point represents the summed predictions of a trace compared to its true label, with transparency set to 0.05 to distinguish point density in overlapping areas.

in the predictions of the $T = 0.3$ model on the test set that are absent in the $T = 0.1$ predictions. This phenomenon exists for several reasons: (1) When using a $T = 0.1$ subdivision, a very high percentage of the images’ true labels have lower class values, and the model that was trained using the $T = 0.1$ window dataset is very accurate for low value classes, whereas a $T = 0.3$ subdivision yields images with higher class values, hence increasing the variance of the true labels, when both models perform worse for the higher value classes as opposed to the lower class value; and (2) any incorrect prediction by either model contributes to an increase in the cumulative predictions for the remainder of the considered trace, thereby *elevating* the overall predicted values.

Both figures show that choosing the optimal window length is difficult and use-case-dependent. While shorter windows improve overall accuracy in cases where an aggregation of images is more important (as seen in this section) and offline analysis is available, longer windows improve the accuracy when examined on a single image (as seen in Section 5). Using shorter windows, however, exacts a higher training and inference cost. Section 5 demonstrates that DecQUIC has the capability to estimate out-of-server-distribution for entire connections.

7 Conclusion

We studied the problem of estimating the number of HTTP/3 responses in a given QUIC connection, acknowledging its impact on network management, load balancing, service quality optimization, and user security. Despite the complexities introduced by the encryption inherent in QUIC connections, as well as the unstable conditions of the internet and user behavior, we successfully estimate the number of responses using DL. We created a dataset of over seven million images from over 100,000 HTTP/3 communication QUIC traces and evaluated the proposed models in two settings: when the web server is known to the observer and when it is unknown. The experiments conducted in both settings achieved remarkably high levels of accuracy, reaching up to 97% CAP accuracy. Furthermore, we demonstrated that the total number of HTTP/3 responses associated with each QUIC connection from over 12,000 traces can be estimated with a very high accuracy of 92.6%.

References

- Sultan Almuhammadi, Abdullatif Alnajim, and Mohammed Ayub. 2023. QUIC Network Traffic Classification Using Ensemble Machine Learning Techniques. *Applied Sciences* 13, 8 (2023), 4725.
- Yuri Sousa Aurelio, Gustavo Matheus De Almeida, Cristiano Leite de Castro, and Antonio Padua Braga. 2019. Learning from imbalanced data sets with weighted cross-entropy function. *Neural processing letters* 50 (2019), 1937–1949.

- Mike Bishop. 2022. HTTP/3. RFC 9114. <https://doi.org/10.17487/RFC9114>
- Mohamed Abdelaziz Chadi Assi, Mohamed Farhan Husain. 2020. QUIC Dataset: A Comprehensive Dataset for QUIC Traffic. <https://www.unb.ca/cic/datasets/quic.html>. Last accessed: July 21, 2024.
- Efstratios Chatzoglou, Vasileios Kouliaridis, Georgios Kambourakis, Georgios Karopoulos, and Stefanos Gritzalis. 2023. A hands-on gaze on HTTP/3 security through the lens of HTTP/2 and a public dataset. *Computers & Security* 125 (2023), 103051.
- Pieter-Tjerk De Boer, Dirk P Kroese, Shie Mannor, and Reuven Y Rubinstein. 2005. A tutorial on the cross-entropy method. *Annals of operations research* 134 (2005), 19–67.
- Rahul Dey and Fathi M Salem. 2017. Gate-variants of gated recurrent unit (GRU) neural networks. In *2017 MWSCAS*. IEEE, IEEE, 1597–1600.
- Eibe Frank and Mark Hall. 2001. A simple approach to ordinal classification. In *ECML 2001: 12th European Conference on Machine Learning*. Springer, Springer, 145–156.
- Ray J Frank, Neil Davey, and Stephen P Hunt. 2001. Time series prediction and neural networks. *JIRS* 31 (2001), 91–103.
- Lisa-Marie Geiginger. 2021. *Classification of Encrypted QUIC Network Traffic*. Ph.D. Dissertation. Wien.
- Ali A. Ghorbani, Wei Lu, and Mahbod Tavallaee. 2012. ISCX Intrusion Detection Evaluation Dataset. <https://www.unb.ca/cic/datasets/ids.html>. Last accessed: July 21, 2024.
- Eyal Horowicz, Tal Shapira, and Yuval Shavitt. 2022. A few shots traffic classification with mini-flowpic augmentations. In *22nd IMC*. 647–654.
- Hassan Ismail Fawaz, Benjamin Lucas, Germain Forestier, Charlotte Pelletier, Daniel F Schmidt, and Weber. 2020. Inceptiontime: Finding alexnet for time series classification. *Data Mining and Knowledge Discovery* 34, 6 (2020), 1936–1962.
- Jana Iyengar and Martin Thomson. 2021. QUIC: A UDP-Based Multiplexed and Secure Transport. RFC 9000. <https://doi.org/10.17487/RFC9000>
- Saadat Izadi, Ahmadi, and Mahmood. 2022a. Network traffic classification using convolutional neural network and ant-lion optimization. *Computers and Electrical Engineering* 101 (2022), 108024.
- Saadat Izadi, Mahmood Ahmadi, and Rajabzadeh. 2022b. Network traffic classification using deep learning networks and Bayesian data fusion. *Journal of Network and Systems Management* 30, 2 (2022), 25.
- Mehak Khan, Hongzhi Wang, and Alladoumbaye Nguetilbaye. 2021. Attention-based deep gated fully convolutional end-to-end architectures for time series classification. *Neural Processing Letters* 53, 3 (2021), 1995–2028.
- Diederik P Kingma and Jimmy Ba. 2014. Adam: A method for stochastic optimization. *arXiv preprint arXiv:1412.6980* (2014).
- Alex Krizhevsky, Ilya Sutskever, and Geoffrey E Hinton. 2012. Imagenet classification with deep convolutional neural networks. *Advances in neural information processing systems* 25 (2012).
- Mirja Kühlewind and Brian Trammell. 2022. Applicability of the QUIC Transport Protocol. RFC 9308. <https://doi.org/10.17487/RFC9308>
- Tsung-Yi Lin, Priya Goyal, and Girshick. 2017. Focal loss for dense object detection. In *IEEE international conference on computer vision*. IEEE, 2980–2988.
- Mohammad Lotfollahi and Jafari Siavoshani. 2020. Deep packet: A novel approach for encrypted traffic classification using deep learning. *Soft Computing* 24, 3 (2020), 1999–2012.
- Jan Luxemburk, Karel Hynek, and Čejka. 2023a. CESNET-QUIC22: A large one-month QUIC network traffic dataset from backbone lines. *Data in Brief* 46 (2023), 108888.
- Jan Luxemburk, Karel Hynek, and Tomáš Čejka. 2023b. Encrypted traffic classification: the QUIC case. In *2023 7th Network Traffic Measurement and Analysis Conference (TMA)*. IEEE, 1–10.
- Kiran Maharana, Surajit Mondal, and Bhushankumar Nemade. 2022. A review: Data pre-processing and data augmentation techniques. *Global Transitions Proceedings* 3, 1 (2022), 91–99.
- Fannia Pacheco, Ernesto Exposito, and Mathieu Gineste. 2020. A framework to classify heterogeneous Internet traffic with Machine Learning and Deep Learning techniques for satellite communications. *Computer Networks* 173 (2020), 107213.
- SGOPAL Patro and Kishore Kumar Sahu. 2015. Normalization: A preprocessing stage. *arXiv preprint arXiv:1503.06462* (2015).

- Jason DM Rennie and Nathan Srebro. 2005. Loss functions for preference levels: Regression with discrete ordered labels. In *IJCAI multidisciplinary workshop*, Vol. 1. AAAI Press, Menlo Park, CA.
- Shahbaz Rezaei and Xin Liu. 2020. Multitask learning for network traffic classification. In *2020 29th ICCCN*. IEEE, 1–9.
- Raffaello Secchi and Cassarà. 2022. Exploring Machine Learning for Classification of QUIC Flows over Satellite. In *ICC 2022 ICC*. IEEE, 4709–4714.
- Robert J. Shahla, Reuven Cohen, and Friedman Roy. 2024. TrafficGrinder: A 0-RTT-Aware QUIC Load Balancer. In *2024 IEEE 32st International Conference on Network Protocols (ICNP)*. IEEE.
- Tal Shapira and Yuval Shavitt. 2019. Flowpic: Encrypted internet traffic classification is as easy as image recognition. In *IEEE 2019 INFOCOM WKSHPS*. IEEE, 680–687.
- Guang-Lu Sun, Yibo Xue, and Dong. 2010. An novel hybrid method for effectively classifying encrypted traffic. In *2010 GLOBECOM*. IEEE, 1–5.
- Junjiao Tian, Niluthpol Chowdhury Mithun, and Seymour. 2020. Recall loss for imbalanced image classification and semantic segmentation. *Neural processing letters* (2020).
- Van Tong and Hai Anh Tran. 2018. A novel QUIC traffic classifier based on convolutional neural networks. In *2018 GLOBECOM*. IEEE, IEEE, 1–6.
- Md Shamim Towhid and Nashid Shahriar. 2022. Encrypted network traffic classification using self-supervised learning. In *2022 NetSoft*. IEEE, 366–374.
- Ashish Vaswani, Noam Shazeer, and Parmar. 2017. Attention is all you need. *Advances in neural information processing systems* 30, 8 (2017), 10.
- Petr Velan, Milan Čermák, and Čeleda. 2015. A survey of methods for encrypted traffic classification and analysis. *International Journal of Network Management* 25, 5 (2015), 355–374.
- Pan Wang, Feng Ye, Xuejiao Chen, and Yi Qian. 2018. Datanet: Deep learning based encrypted network traffic classification in sdn home gateway. *IEEE Access* 6 (2018), 55380–55391.
- Qi Wang, Yue Ma, Kun Zhao, and Yingjie Tian. 2020. A comprehensive survey of loss functions in machine learning. *Annals of Data Science* (2020), 1–26.

A Appendices

Table 5: $T = 0.1$ -second window dataset: Images per class value, per server.

| Class | youtube.com | semrush.com | discord.com | instagram.com | mercedes-benz.com | bleacherreport.com | nicelocal.com | facebook.com | pcmag.com | logitech.com | google.com | cdnetworks.com | independent.co.uk | cloudflare.com | jetbrains.com |
|-------|-------------|-------------|-------------|---------------|-------------------|--------------------|---------------|--------------|-----------|--------------|------------|----------------|-------------------|----------------|---------------|
| 0 | 68,730 | 113,947 | 190,942 | 10,340 | 4,255 | 421,728 | 113,581 | 9,345 | 996,908 | 14,435 | 37,501 | 40,332 | 126,199 | 417,474 | 10,993 |
| 1 | 32,180 | 137,842 | 156,369 | 2,958 | 1,154 | 190,606 | 103,038 | 4,303 | 141,714 | 14,785 | 18,567 | 50,600 | 37,183 | 506,356 | 5,392 |
| 2 | 13,426 | 53,672 | 126,360 | 1,215 | 661 | 39,619 | 119,751 | 2,219 | 29,480 | 9,181 | 7,584 | 39,329 | 6,004 | 192,943 | 4,285 |
| 3 | 7,961 | 32,087 | 63,141 | 621 | 523 | 19,860 | 71,226 | 1,374 | 4,330 | 4,206 | 4,637 | 21,876 | 1,890 | 121,638 | 2,202 |
| 4 | 5,733 | 23,880 | 37,571 | 314 | 449 | 33,013 | 42,885 | 922 | 2,996 | 5,166 | 3,899 | 14,017 | 1,138 | 54,700 | 1,579 |
| 5 | 9,184 | 17,406 | 21,260 | 359 | 442 | 20,144 | 28,455 | 349 | 2,145 | 1,620 | 2,484 | 8,940 | 811 | 33,681 | 1,692 |
| 6 | 1,210 | 10,376 | 8,374 | 472 | 443 | 14,649 | 18,191 | 545 | 2,429 | 1,238 | 1,576 | 6,523 | 1,129 | 16,264 | 1,811 |
| 7 | 751 | 7,981 | 5,235 | 338 | 281 | 9,473 | 16,304 | 4,143 | 1,788 | 719 | 1,572 | 4,522 | 522 | 3,397 | 1,154 |
| 8 | 488 | 7,624 | 3,342 | 171 | 339 | 17,508 | 12,342 | 336 | 813 | 338 | 998 | 3,417 | 383 | 987 | 1,616 |
| 9 | 111 | 7,292 | 2,757 | 140 | 237 | 3,735 | 11,027 | 324 | 339 | 417 | 493 | 2,421 | 290 | 326 | 2,635 |
| 10 | 39 | 8,132 | 2,251 | 66 | 209 | 7,510 | 10,050 | 383 | 213 | 348 | 345 | 2,040 | 240 | 195 | 745 |
| 11 | 14 | 8,308 | 1,143 | 9 | 171 | 2,587 | 5,406 | 275 | 249 | 370 | 297 | 1,847 | 171 | 165 | 764 |
| 12 | 9 | 5,557 | 1,264 | 0 | 145 | 272 | 2,861 | 289 | 84 | 801 | 261 | 1,706 | 163 | 98 | 66 |
| 13 | 11 | 5,109 | 768 | 0 | 129 | 230 | 1,397 | 332 | 148 | 462 | 200 | 1,569 | 123 | 113 | 0 |
| 14 | 7 | 4,211 | 683 | 0 | 151 | 270 | 736 | 136 | 8 | 717 | 218 | 1,289 | 108 | 80 | 0 |
| 15 | 4 | 4,964 | 685 | 0 | 91 | 184 | 342 | 313 | 5 | 464 | 146 | 1,415 | 109 | 96 | 0 |
| 16 | 6 | 6,328 | 318 | 0 | 68 | 201 | 123 | 48 | 41 | 473 | 169 | 1,437 | 68 | 74 | 0 |
| 17 | 8 | 6,029 | 311 | 0 | 83 | 176 | 125 | 55 | 18 | 441 | 99 | 1,229 | 64 | 55 | 0 |
| 18 | 4 | 5,442 | 348 | 0 | 83 | 73 | 87 | 26 | 21 | 221 | 77 | 1,014 | 65 | 41 | 0 |
| 19 | 8 | 4,797 | 271 | 0 | 40 | 47 | 31 | 56 | 8 | 211 | 76 | 998 | 38 | 16 | 0 |
| 20 | 5 | 3,732 | 430 | 0 | 33 | 30 | 23 | 36 | 1 | 141 | 44 | 1,152 | 42 | 26 | 0 |
| Sum | 139,889 | 474,716 | 623,823 | 17,003 | 9,987 | 781,915 | 857,981 | 25,999 | 1,183,738 | 86,754 | 81,243 | 207,673 | 176,740 | 1,347,725 | 34,934 |

Table 6: $T = 0.3$ -second window dataset: Images per class value, per server.

| Class | youtube.com | semrush.com | discord.com | instagram.com | mercedes-benz.com | bleacherreport.com | nicelocal.com | facebook.com | pcmag.com | logitech.com | google.com | cdnetworks.com | independent.co.uk | cloudflare.com | jetbrains.com |
|------------|---------------|----------------|----------------|---------------|-------------------|--------------------|----------------|---------------|----------------|---------------|---------------|----------------|-------------------|----------------|---------------|
| 0 | 11,185 | 23,751 | 26,130 | 2,942 | 1,082 | 107,871 | 19,851 | 1,537 | 316,252 | 3,990 | 7,031 | 8,530 | 31,494 | 45,521 | 3,100 |
| 1 | 12,954 | 56,849 | 22,566 | 1,081 | 214 | 70,024 | 21,724 | 1,510 | 35,476 | 5,041 | 6,702 | 13,318 | 26,392 | 86,815 | 1,713 |
| 2 | 6,509 | 34,403 | 21,911 | 655 | 168 | 37,090 | 23,963 | 640 | 21,239 | 4,439 | 4,465 | 11,463 | 4,968 | 84,493 | 1,622 |
| 3 | 4,651 | 18,272 | 33,139 | 359 | 105 | 18,401 | 23,611 | 917 | 5,272 | 2,663 | 1,954 | 7,993 | 2,075 | 37,014 | 1,005 |
| 4 | 3,447 | 13,116 | 33,214 | 286 | 78 | 11,685 | 18,049 | 768 | 1,427 | 2,261 | 1,617 | 7,114 | 928 | 22,280 | 722 |
| 5 | 6,307 | 12,567 | 23,249 | 143 | 71 | 7,682 | 15,305 | 312 | 768 | 1,629 | 912 | 6,084 | 491 | 14,270 | 732 |
| 6 | 3,745 | 7,098 | 17,279 | 237 | 88 | 6,711 | 12,300 | 167 | 1,077 | 2,182 | 860 | 5,844 | 292 | 13,965 | 741 |
| 7 | 2,918 | 5,823 | 18,919 | 341 | 67 | 8,433 | 9,786 | 2,254 | 1,114 | 759 | 1,293 | 5,140 | 363 | 12,438 | 522 |
| 8 | 1,439 | 4,921 | 13,591 | 238 | 76 | 22,045 | 8,065 | 193 | 1,047 | 511 | 979 | 4,414 | 246 | 10,979 | 1,025 |
| 9 | 815 | 3,624 | 4,322 | 189 | 71 | 12,548 | 7,170 | 63 | 468 | 477 | 529 | 3,350 | 153 | 7,975 | 1,642 |
| 10 | 230 | 3,917 | 2,848 | 190 | 78 | 13,965 | 7,394 | 69 | 358 | 342 | 370 | 2,717 | 117 | 2,784 | 1,505 |
| 11 | 166 | 5,221 | 1,651 | 167 | 62 | 10,530 | 7,527 | 61 | 551 | 335 | 396 | 2,024 | 173 | 954 | 2,383 |
| 12 | 80 | 4,704 | 1,261 | 77 | 50 | 2,464 | 8,338 | 114 | 267 | 360 | 373 | 1,754 | 103 | 641 | 1,677 |
| 13 | 46 | 3,430 | 882 | 7 | 50 | 478 | 9,361 | 185 | 103 | 289 | 317 | 1,336 | 125 | 443 | 71 |
| 14 | 24 | 2,194 | 988 | 0 | 66 | 248 | 10,034 | 713 | 169 | 982 | 274 | 1,055 | 110 | 290 | 0 |
| 15 | 29 | 2,725 | 775 | 0 | 71 | 341 | 7,660 | 293 | 75 | 549 | 273 | 909 | 133 | 152 | 0 |
| 16 | 14 | 3,827 | 669 | 0 | 62 | 232 | 5,217 | 192 | 25 | 444 | 188 | 752 | 58 | 125 | 0 |
| 17 | 10 | 4,288 | 431 | 0 | 60 | 369 | 3,471 | 185 | 33 | 516 | 169 | 626 | 51 | 88 | 0 |
| 18 | 10 | 3,641 | 479 | 0 | 75 | 170 | 2,207 | 356 | 50 | 387 | 152 | 469 | 71 | 93 | 0 |
| 19 | 11 | 3,300 | 408 | 0 | 77 | 104 | 1,177 | 424 | 14 | 262 | 132 | 375 | 78 | 80 | 0 |
| 20 | 9 | 3,806 | 536 | 0 | 69 | 139 | 759 | 35 | 12 | 162 | 82 | 440 | 59 | 48 | 0 |
| Sum | 54,659 | 221,477 | 235,248 | 7,112 | 2,740 | 331,530 | 222,969 | 10,988 | 385,797 | 28,580 | 29,068 | 85,707 | 68,480 | 341,488 | 18,470 |